processes

MDPI

Article

Removal of Fluoroquinolone Antibiotics by Chitosan–Magnetite from Aqueous: Single and Binary Adsorption

Quy M. Bui [1,*], Tung Q. Vu [1], Xuan T. Vuong [1], Vinh D. Nguyen [1], Linh T. N. Nguyen [1], Ha T. Le [2], Hoa T. H. Nguyen [1] and Van Phuoc Nguyen [3,4,*]

[1] Faculty of Chemistry, TNU-University of Sciences, Thai Nguyen 250000, Vietnam; tungvq@tnus.edu.vn (T.Q.V.); xuanvt@tnus.edu.vn (X.T.V.); vinhnd@tnus.edu.vn (V.D.N.); linhntn@tnus.edu.vn (L.T.N.N.); hoanth@tnus.edu.vn (H.T.H.N.)
[2] Institute of Sciences and Technology, TNU-University of Sciences, Thai Nguyen 250000, Vietnam; halt@tnus.edu.vn
[3] NTT Institute of Applied Technology and Sustainable Development, Nguyen Tat Thanh University, Ho Chi Minh City 70000, Vietnam
[4] Faculty of Environmental and Food Engineering, Nguyen Tat Thanh University, Ho Chi Minh City 70000, Vietnam
* Correspondence: quybm@tnus.edu.vn (Q.M.B.); nvphuoc@ntt.edu.vn (V.P.N.)

Abstract: In this research, chitosan–magnetite composites (CS-MNPs) were successfully synthesized using a rapid and easy technique. The materials were characterized by FTIR, XRD, EDX, TEM, VSM, and BET methods. The removal of the antibiotics ciprofloxacin (CFX) and levofloxacin (LFX) from aqueous solutions by CS-MNPs adsorbent was investigated. The influencing factors in a single adsorption system were studied, including pH (1–11), initial concentration (2.5–15.0 mg/L), contact time (0–120 min), and adsorbent dosage (5–50 mg/L). The experiment data were analyzed by pseudo-first-order and pseudo-second-order kinetic models. The adsorption isotherms were studied by fitting the experimental data to the Langmuir, Freundlich, and Temkin models. The results indicated that the adsorption of CFX and LFX antibiotics was consistent with the pseudo-second-order kinetics model, the Langmuir isotherm model. Binary adsorption systems (CFX: LFX) with concentration ratios of 1:0, 1:0.5, 1:1.0, 1:1.5, and 1:2.0 were also studied. The antibiotics CFX and LFX were absorbed by CS-MNPs simultaneously in the aqueous solution. The presence of the second component in the solution reduced the first component's ability to adsorb. The adsorption process in the binary system followed the Langmuir competition model. After four regenerations, CS-MNPS exhibited stability and was well reusable. Studies on actual samples showed that CS-MNPs could effectively remove FQs from those samples, with a treatment efficiency of above 98%.

Keywords: chitosan; magnetite; ciprofloxacin; levofloxacin; adsorption; binary

Citation: Bui, Q.M.; Vu, T.Q.; Vuong, X.T.; Nguyen, V.D.; Nguyen, L.T.N.; Le, H.T.; Nguyen, H.T.H.; Nguyen, V.P. Removal of Fluoroquinolone Antibiotics by Chitosan–Magnetite from Aqueous: Single and Binary Adsorption. *Processes* **2023**, *11*, 2396. https://doi.org/10.3390/pr11082396

Academic Editor: Maria Jose Martin de Vidales

Received: 18 June 2023
Revised: 17 July 2023
Accepted: 19 July 2023
Published: 9 August 2023

1. Introduction

Fluoroquinolone (FQ) antibiotics, a group of medicines that treat bacterial infections in people, have received more focus in recent years because of their harmful effects on both human and aquatic ecosystems [1–3]. Due to their lengthy conversion durations and low degradation efficiency, FQs such as ciprofloxacin (CFX) and levofloxacin (LFX) are widely disseminated in surface waters [4–7]. Antibiotics present several potentially significant hazards for humans and ecosystems by causing the growth and spread of antibiotic resistance in bacteria and leading to the potential of antimicrobial resistance [8,9]. Therefore, it is necessary to remove antibiotics from the aqueous solution. Many methods applied to remove antibiotics have been studied. Adsorption [10–12], coagulation [13], biological treatment [14,15], photocatalytic degradation [16], and advanced oxidation [17,18] are common FQs treatment methods. Due to its low cost, high treatment efficiency, environmental friendliness, and simplicity of use, the adsorption method is regarded as one of the best

and most promising approaches [19–21]. Therefore, the selection of suitable adsorbent materials has been studied by scientists.

Recently, the scientific community has directed some advanced research in the development of alternative adsorbents, especially those based on polymers. Chitosan is a biopolymer extracted from crustaceans' shells. Chitosan has several benefits, including simplicity in synthesis, economy, and environmental friendliness [22]. Chitosan is frequently applied to remove pollutants from aqueous solutions because of the molecule's hydroxyl and amine functional groups [22–25]. Chitosan, however, has several restrictions and drawbacks, including low solubility, low mechanical strength, and difficulty recovering the material after usage [22]. Thus, altering or functionalizing chitosan to improve its characteristics has emerged as a critical method for conducting practical research on chitosan [24,26,27]. The focus of the study on adsorption has changed to the synthesis of materials with magnetic properties by mixing chitosan with magnetic compounds (such as Fe, Mn, Co, etc.). This improves the mechanical strength and adsorption capacity and makes reusing the adsorbent easier [28–31]. Chitosan–magnetite (CS-MNPs) is a biological composite that combines chitosan and Fe_3O_4. Many advantages of CS-MNPs included their easy synthesis, substantial surface area, and environmental friendliness. In addition, with the existence of Fe_3O_4 in the material, CS-MNPs were effortlessly recovered by the magnetic field of the magnet. Therefore, CS-MNPs have been used commonly in environmental treatments such as dyes, heavy metal ions, and antibiotics [28,31–36]. However, previous publications were only interested in eliminating single common antibiotics from water, such as ciprofloxacin, amoxicillin, norfloxacin, moxifloxacin, ofloxacin, tetracycline, and paracetamol [37–39]. The applicability of adsorbent materials in practice has also rarely been mentioned by researchers [37,40]. Furthermore, research on the adsorption of LFX antibiotics by CS-MNPs has not yet been reported. There have also been no studies using binary systems to study the simultaneous removal of CFX and LFX from aqueous solutions, although, in practice, wastewater frequently consists of a complex mixture of components. Since there may be some interaction and competition between two or more components for adsorption sites, it is vital to research the adsorption potential and selectivity of the adsorbent to remove antibiotic residues in a multi-component system [41,42].

Therefore, in this study, CS-MNP materials were rapidly and straightforwardly synthesized by in situ methods combined with co-precipitation. The material properties were determined by FTIR, XRD, EDS, TEM, VSM, and BET methods. The synthesized materials were used to study the adsorption of CFX and LFX antibiotics on single and binary systems. Factors affecting the adsorption process, such as pH, initial antibiotic concentration, adsorption time, and adsorbent dosage, were studied. Experimental data were analyzed for isotherm adsorption models (Langmuir, Freundlich, and Temkin), kinetic adsorption models (pseudo-first-order and pseudo-second-order), and Langmuir competition models. The reuse of CS-MNPs and the adsorption mechanism were also presented in this paper. The ability of CS-MNPs for environmental remediation was investigated in actual contaminated water samples collected at aquaculture farms.

2. Materials and Methods

2.1. Chemicals

Ciprofloxacin (CFX, $C_{17}H_{18}FN_3O_3{\cdot}HCl$, purity > 93%) and levofloxacin (LFX, $C_{18}H_{20}FN_3O_4$, purity > 98.5%) were purchased from the National Institute of Drug quality control, Viet Nam. Other chemicals used in the study (including $FeCl_2{\cdot}4H_2O$ (98%), $FeCl_3{\cdot}6H_2O$ (98.5%), NaOH (>98%), CH_3COOH (>99%), HCl (35–36.5%), NaOH (>98%), and chitosan (85% DD) were obtained from Sigma-Aldrich Chemical Co. (Burlington, MA, USA), Xinlong (Shouguang, China), and Merck, (KGaA, Darmstadt, Germany)). They were all guaranteed to be of chemical purity used in the analysis. All of the tests were carried out using double-distilled water.

2.2. Synthesis Adsorbate Materials

CS-MNPs nanoparticles were prepared based on the previous report [43]. The material was synthesized with a CS:MNPs mass ratio of 4:6. The first, 20 mL of a solution containing Fe^{3+} (0.5 M) and Fe^{2+} (0.25 M), were added to 20 mL of a CS solution, which was made by dissolving 3.48 g of CS in 30 mL of 2% acetic acid, at 70 °C under N_2 atmosphere. This prevents the oxidization of Fe^{2+} by oxygen in the air. The reaction system was continuously and vigorously stirred at 1500 rpm. A solution of NaOH 2 M was added until the pH of the reaction system was 13. After that, the system was kept under these conditions for 50 min. Finally, the synthesized materials were separated from the liquid by using a magnet, washed with distilled water until the pH of the washed water reached 7, and dried at 70 °C for 24 h.

2.3. Characterization

Fourier transform infrared spectroscopy (FTIR) with KBr pellets using the FTIR 4600 Jasco spectrum (Tokyo, Japan) under dry air conditions at room temperature was applied to determine the functional groups of CS-MNPs nanoparticles. The crystalline structure of the materials was analyzed by X-ray diffraction (XRD, D2-Phase, Bruker, Karlsruhe, Germany) with 2 theta angles in a range of 10–70°. The composition of the materials was analyzed on an energy-dispersive X-ray spectrometer (EDX, Jeol 5410, Tokyo, Japan) in the energy range of 0–16.5 keV. Scanning electron microscope (SEM, FE-SEM Hitachi S-4800, Japan) and Transmission electron microscopy (TEM, Jeol 200CX, Tokyo, Japan) at 100 keV were used to determine the shape and size of CS-MNPs. The magnetic properties of CS-MNPs were measured with a vibrating sample magnetometer (VSM, Lake Forest, CA, USA) at ±10 kOe and 25 °C. The surface area, pore size, and volume of CS-MNPs nano adsorbents and components were determined by nitrogen gas adsorption and absorption analysis (BET, Tri Star II, Norcross, GA, USA).

To determine the zero surface charge of the synthesized nanoparticles (pH_{zpc}), 0.02 g of the synthesized nanoparticles was first added to 20 mL of a 0.1 M sodium chloride solution. Then, we adjusted the pH from 1.0 to 13.0 with HCl (0.1 N) or NaOH (0.1 N) solutions. These solutions were then stirred at room temperature at a rate of at least 1500 rpm for 24 h. Finally, the pH of these solutions was determined using a pH meter. The zero charge point was obtained from the plot of initial pH_1 vs. ΔpH (change in pH).

2.4. Adsorption Experiments

2.4.1. Single Adsorption

Solution pH, contact time, initial antibiotic concentration, and adsorbent dose were the variables to be studied when investigating the adsorption ability of CFX and LFX antibiotics onto CS-MNPs. The studies were conducted under set parameters: 293 K, 1500 rpm stirring, and 25 mL solution. Each experiment was repeated three times, and the average value was taken. Table 1 summarizes additional experimental parameters for each experiment.

Table 1. The experimental parameters.

Experiment/Parameters	pH	Time (min)	CS-MNPs Mass (mg)	Initial Concentration (mg/L)
Effect of pH	1–11	30	20	10.15
Effect of time/initial concentration	7	5 to 120	20	2.50 to 15.00
Effect of dosage	7	60	5–50	10

Effect of pH: The impact of pH on adsorption was investigated by placing 20 mg of dry CS-MNPs in a series of flasks containing 25 mL of solution antibiotics (10.15 mg/L) with different pH values (from 1 to 11), stirring at 1500 rpm and 293 K for 30 min, and separating CS-MNPs. The residual antibiotic concentration was measured by UV-Vis measured.

Effect of time and initial antibiotic concentration: A 25 mL solution of antibiotic concentration (2.5, 5.0, 10.0, and 15.0 mg/L), with pH 7, was placed in a series of flasks containing 20 mg of dried CS-MNPs and then stirred at 1500 rpm and 293 K. After each interval (5, 10, 15, 20, 30, 60, 90, 120, and 150 min), determine the antibiotic concentration after adsorption.

Effect of dosage: Seven different weights (5, 10, 15, 20, 25, 30, and 50 mg) of dried CS-MNPs were enclosed in a series of flasks, each of which contained 25 mL of antibiotics (10 mg/L), pH 7, then stirred at 1500 rpm and 293 K. After 60 min, the CS-MNPs were separated from the solution using the magnetic field of the magnet, and then the concentration of residual antibiotic in the solution was determined.

After each adsorption test, place a magnet adjacent to the flask containing the research solution. Because CS-MNPs are magnetic materials, they were rapidly attracted to the magnet. As a result, the adsorbent solution conveniently took out of the mixture. Therefore, filter papers were not required to separate the particles from the solution. This is one of the benefits of employing magnetic materials in this adsorption research.

The antibiotic removal efficiency and adsorption capacity at t time and equilibrium time were determined according to Equations (1)–(3), respectively.

$$RE = \frac{(C_0 - C_t) \cdot 100}{C_0} \quad (1)$$

$$q_e = \frac{(C_0 - C_t) \cdot V}{m} \quad (2)$$

$$q_t = \frac{(C_0 - C_t) \cdot V}{m} \quad (3)$$

where: C_0, C_e, and C_t are the initial, equilibrium, and at t time concentration (mg/L) of antibiotic in solution, respectively; RE is the adsorption efficiency; q_e and q_t (mg/g) are the equilibrium and at t time adsorption capacity; m (g) is the weight of the adsorbent; and V (L) is the volume of the solution.

The concentrations of CFX and LFX before and after adsorption were determined on a UV-Visible spectrometer (UV-Vis, Jasco V-770, Tokyo, Japan) at a wavelength of 275 nm and 294 nm, respectively.

2.4.2. Binary Adsorption

Two research systems have been established: (CFX: LFX) and (LFX: CFX). It maintains the original concentration of the first antibiotic in each system while varying the amount of the remaining antibiotic in the system based on the concentration ratios of 1:0, 1:0.5, 1:1, 1:1.5, and 1:2. C_0 = 2.51 and 5.13 mg/L were the initial antibiotic concentrations used in the investigation. Experiments were conducted at a fixed condition of 25 mL of research solution, pH 7, 60 min, 20 mg CS-MNPs, and 293 K. According to Equations (1) and (2), estimate the effectiveness of antibiotic removal and adsorption capacity. The experiments were carried out three times, and the average result was calculated. The average error for each experiment was around 5%.

2.5. Regeneration Study

The reusability of the CS-MNPs adsorbent was investigated by adsorption–regeneration studies. The used adsorbent was regenerated by shaking with 25 mL of NH_3 solution (0.5 N) for 60 min, then magnetically separated, washed three times with deionized water, and dried for 24 h at 70 °C. The regenerated adsorbent was used for CFX and LFX adsorption under similar conditions to the initial one. This regeneration–adsorption experiment was repeated four times (cycles 1, 2, 3, and 4). After each adsorption–desorption cycle, the final concentrations of antibiotic solutions were determined using the same procedure described in Section 2.4.1

3. Results

3.1. Characterization of Material

The XRD spectrum results of CS-MNPs (Figure 1) show that the characteristic peaks of MNPs appear on the diagram at positions 2 theta = 30.1°, 35.5°, 43.1°, 53.1°, 57.3°, and 62.7°, which are corresponded to the planes (220), (311), (400), (422), (511), and (422), respectively. This is the cubic spinel structure of MNPs [35]. On the diagram of CS-MNPs, chitosan characteristics also appear at position 2θ = 20.4° [36]. This proves that CS-MNPs materials have been successfully synthesized and that the synthesis process does not change the phase of MNPs [28,29,32]. The synthesized CS-MNPs have a cubic spinel structure.

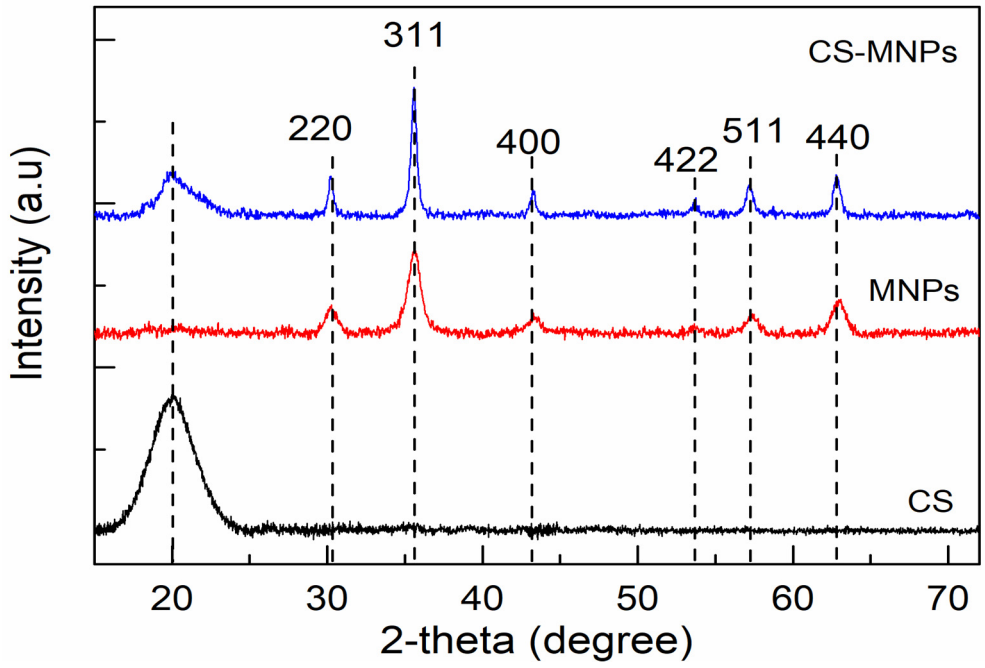

Figure 1. The XRD patterns of CS, MNPs, and CS-MNPs.

The FTIR spectra of CS, MNPs, and CS-MNPs are shown in Figure 2. The broad band at 3435 cm^{-1} in the CS spectrum corresponds to the O-H stretching overlapping the N-H stretching, while the band at 3019 cm^{-1} was attributed to the C-H stretching. They were shifted to positions 3279 and 2882 cm^{-1} on the spectrum of CS-MNPs. Furthermore, in the spectra of CS-MNPs, compared with that of MNPs, the peaks at about 628 cm^{-1} and 580 cm^{-1} corresponding to the Fe-O bond [35] shifted to 624 cm^{-1} and 547 cm^{-1}. In addition, on the spectrum of CS-MNPs, spectral peaks also appear at positions 1645 cm^{-1}, 1545 cm^{-1}, and 1407 cm^{-1}, assigned to C=O stretching vibration of amide, bending vibration of N-H, and C-H in the chitosan molecule, respectively. The peak of 1070 cm^{-1} is associated with the stretching vibration in the C-OH of chitosan [36,44–46]. The position of absorption peaks had a slight shift between chitosan and CS-MNPs, mainly due to the complexation of Fe^{3+} with the amino and hydroxyl groups of chitosan [28].

Analysis of energy-dispersive X-ray (EDX) spectroscopic of CS-MNPs reveals the presence of iron, oxygen, and carbon components in CS-MNPs nanocomposites (Figure 3). The elemental percentage composition of iron, oxygen, and carbon is 17.66, 61.83, and 20.51%, respectively. That corresponds with the mass composition of CS and MNPs being 38.71 and 61.29%, respectively, and the mass ratio of CS: MNPs in the material being approximately 4:6. This result is consistent with the CS-MNPs synthesis method used (Section 2.2). No other peak related to any impurity has been detected in the EDS, which confirmed that the grown CS-MNPs nanoparticles in the nanocomposite strip are composed only of iron, oxygen, and carbon.

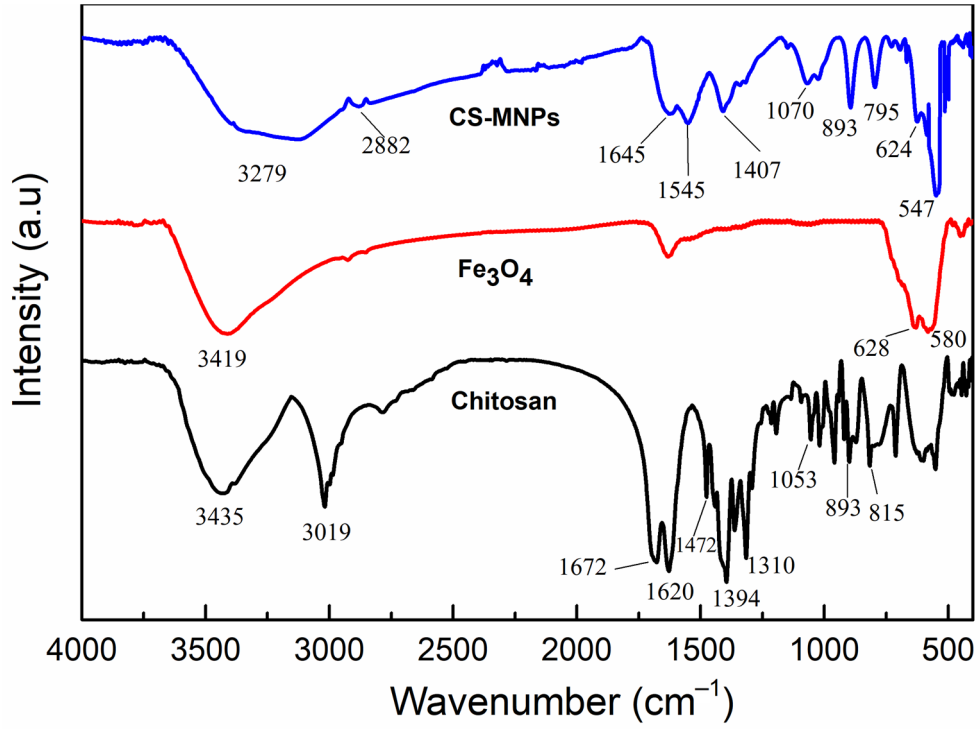

Figure 2. The FTIR spectra of CS, MNPs, and CS-MNPs.

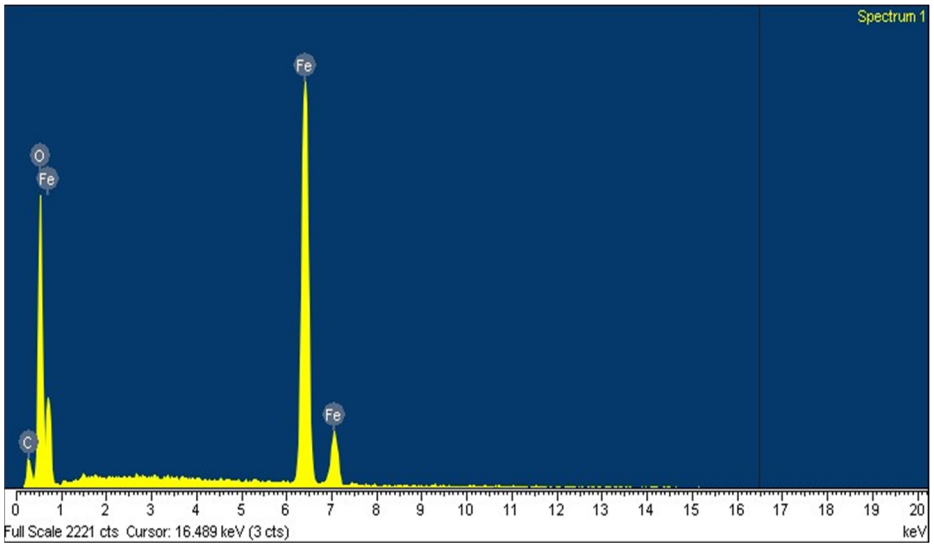

Figure 3. The EDX pattern of CS-MNPs.

The morphology of the CS-MNPs is shown by the SEM and TEM image results (Figure 4). It can be seen that the synthesized CS-MNPs had a porous surface and existed in a spherical shape with a diameter of about 20 nm. CS-MNPs had a saturation magnetism of 46.2 emu/g, smaller than the individual MNPs (75.1 emu/g) (Figure 5). This result can be clarified that CS was a non-magnetic material, and when combined with MNPs, it reduced the magnetism of the material. The value from the saturation of these CS-MNPs was quite large, more significant than that reported by A. Kadam et al. and G. Li et al. (21 emu/g) [28,47]. Thus, the CS-MNPs material can be straightforwardly recovered after adsorption by using the magnetic field of the magnet.

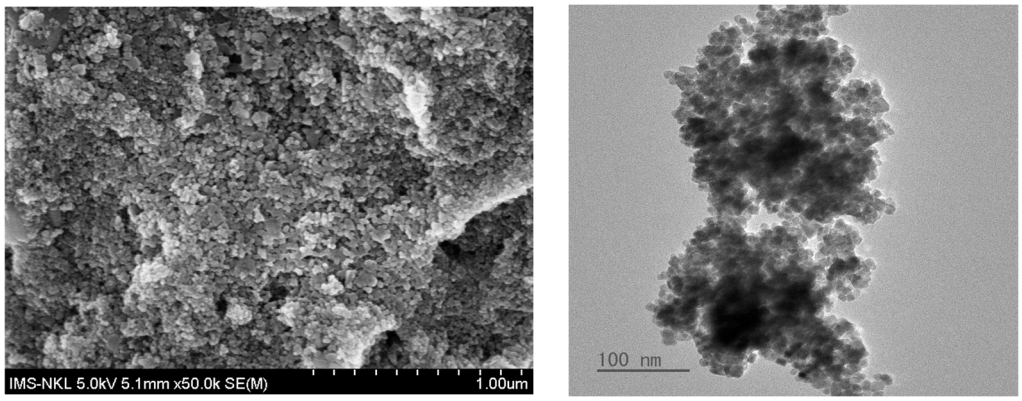

Figure 4. The SEM (**left**) and TEM (**right**) images of CS-MNPs.

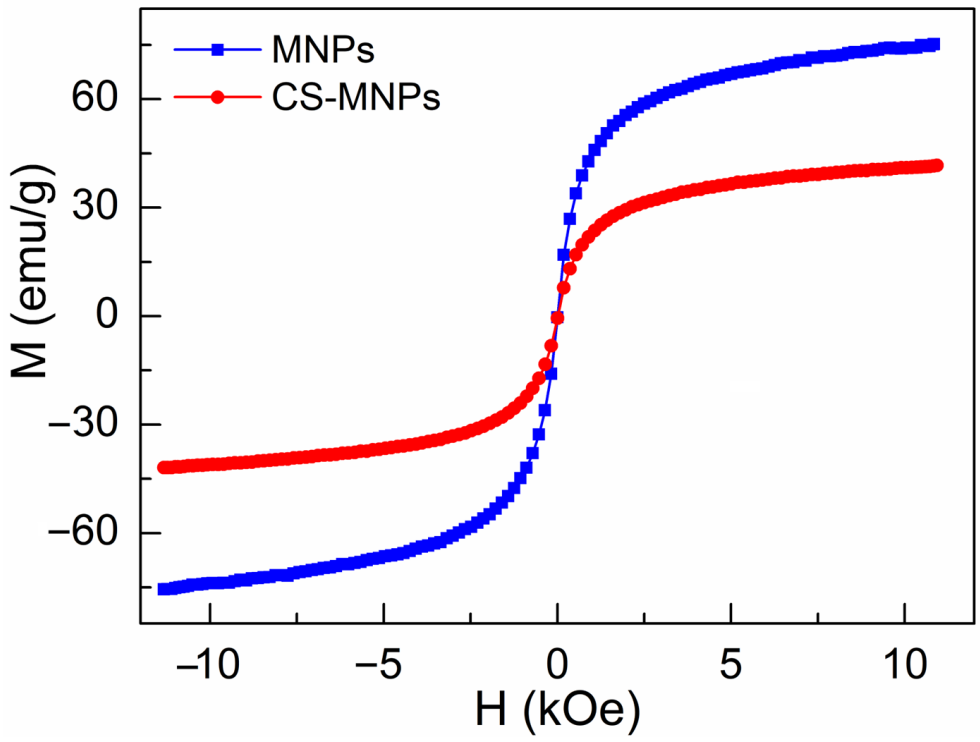

Figure 5. The magnetic hysteresis curves of MNPs and CS-MNPs.

The surface area of CS-MNPs (Table 2) with a value of 79.60 m^2/g was determined using N_2 adsorption isotherms. This value is several times larger than the surface area of chitosan alone (3.75 m^2/g) and smaller than that of MNPs (90.33 m^2/g). This can be explained because chitosan is a polymeric material with high viscosity, so it has masked the surface of MNPs during the synthesis of CS-MNPs [48].

Table 2. Analysis of BET.

Parameters	CS	MNPs	CS-MNPs
Surface (m^2/g)	3.75	90.33	79.60
Average pore size (nm)	18.39	17.75	8.43
Pore volume (cm^3/g)	0.02	0.42	0.17

3.2. Single Adsorption of CFX and LFX Antibiotic

3.2.1. Determination of Adsorption Ability

The removal effectiveness of CFX and LFX from each material (CS, MNPs, and CS-MNPs) was investigated to compare the ability adsorption of the adsorbents. Experiments were conducted at room temperature, pH = 7, an initial concentration of 5.0 mg/L, and an adsorption duration of 120 min. Experiments were performed three times and averaged. Figure 6's outcome demonstrates that the synthetic composite material had a greater efficiency for removing antibiotics than either CS or MNPs individually. The increased active sites, the stability of the CS-MNPs composites, and the synergistic interaction between CS and MNPs might all have contributed to this outcome. These experimental results led to the selection of CS-MNPs materials for application study in removing antibiotics from the aqueous solution.

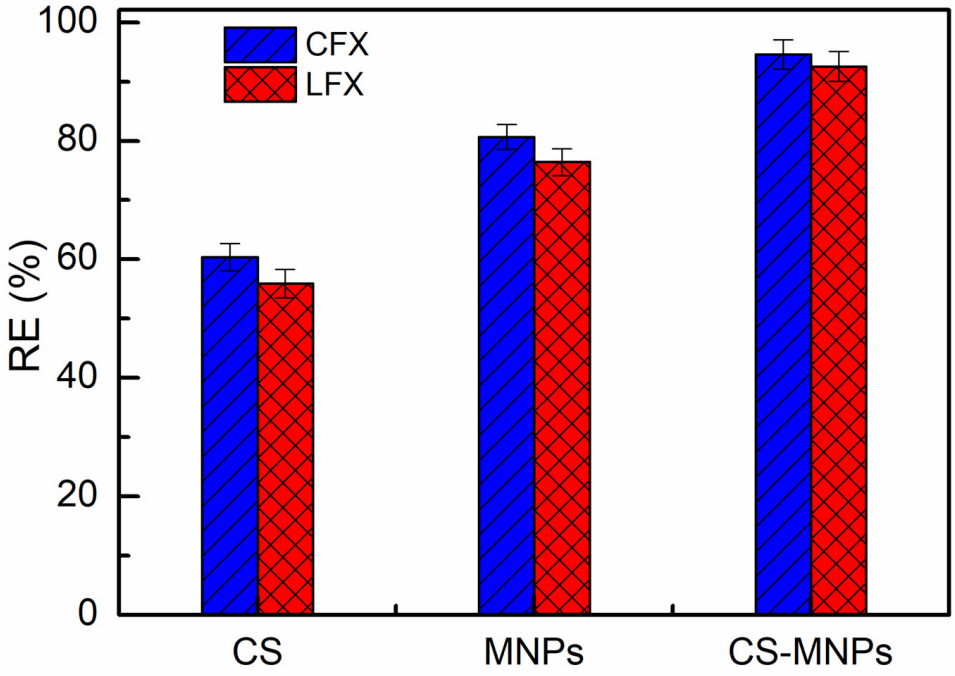

Figure 6. The remove efficiency CFX and FLX antibiotics of three adsorbents (experimental conditions: m = 20 mg, V = 20 mL, time = 120 min, and T = 293 °C, n = 3).

3.2.2. Effect of pH

The ionization of the adsorbent and the surface of the adsorbent are influenced by the pH of the solution. The dissociation constants of CFX and LFX determine whether or not they are present in the solution (CFX: pK_{a1} = 5.9, pK_{a2} = 8.89 [49], LFX: pK_{a1} = 6.02, pK_{a2} = 8.15 [19]). Antibiotics exist in cationic form (CFX^+, LFX^+) at pH < pK_{a1}. Antibiotics exist in anionic form when pH > pK_{a2} (CFX^-, LFX^-). The antibiotics exist in the zwitterionic form ($CFX^{\pm}$, $LFX^{\pm}$) between pK_{a1} and pK_{a2} of pH. Chitosan had a zero change point (pH_{pzc}) of 4.6 [50], while MNPs had a pH_{pzc} of 6.55 [51], and CS-MNPs had a pH_{pzc} of around 6.5 (Figure 7). This indicates that the presence of MNPs in the material significantly impacted the pH_{pzc} of CS-MNPs. In other words, the material's surface had a positive charge when the solution pH < pH_{pzc} and a negative charge when the pH > pH_{pzc}. The antibiotic adsorption ability of CS-MNPs can be significantly impacted by this value.

Figure 8 shows that the ability to remove CFX and LFX increased as pH rose from 1 to 7, peaking at pH = 7 (RE_{CFX} = 79.7%; RE_{LFX} = 69.85%), after which the effectiveness of antibiotic removal significantly reduced as solution pH rose from 8 to 11. The change in the adsorbent's molecular charge in the solution can account for this. At pH 7, CFX and LFX exist in their zwitterionic forms ($CFX^{\pm}$, $LFX^{\pm}$), while on the surface of CS-MNPs exist negatively charged functional groups, such as O^{2-} of MNPs and hydroxyl –OH of chitosan

and MNPs. As a result, electrostatic attraction between $CFX^{\pm}$/$LFX^{\pm}$ and the negatively charged surface of CS-MNPs occurs, and the effectiveness of antibiotics increases. Thus, this study selected a pH of 7 as the optimal adsorption condition for the CFX and LFX.

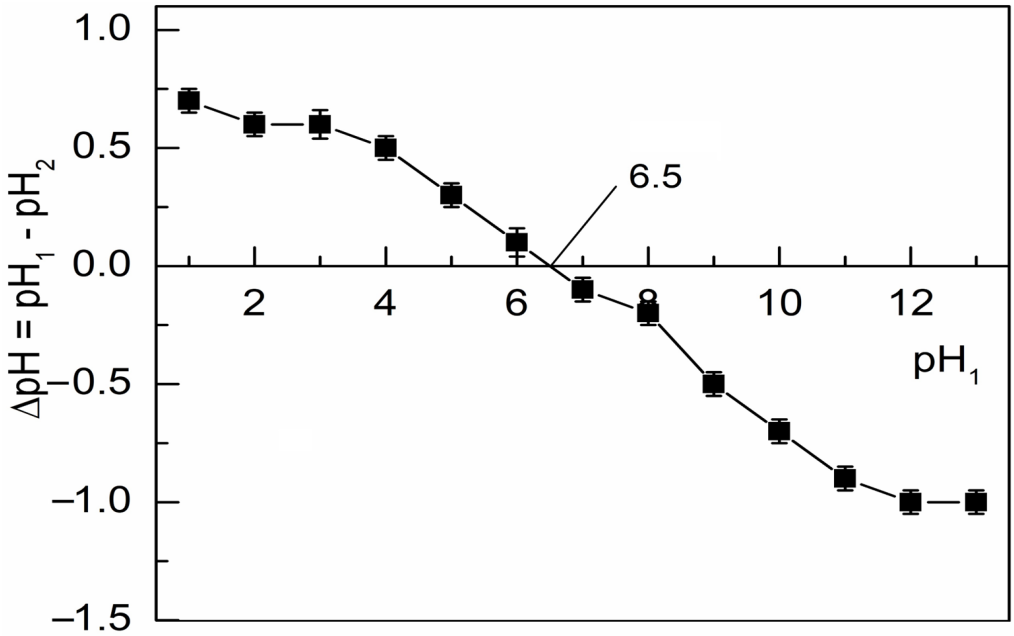

Figure 7. The zero surface charge of CS-MNPs (experimental conditions: m = 20 mg, V = 20 mL, time = 24 h, and T = 293 °C; mean ± 0.05, n = 3).

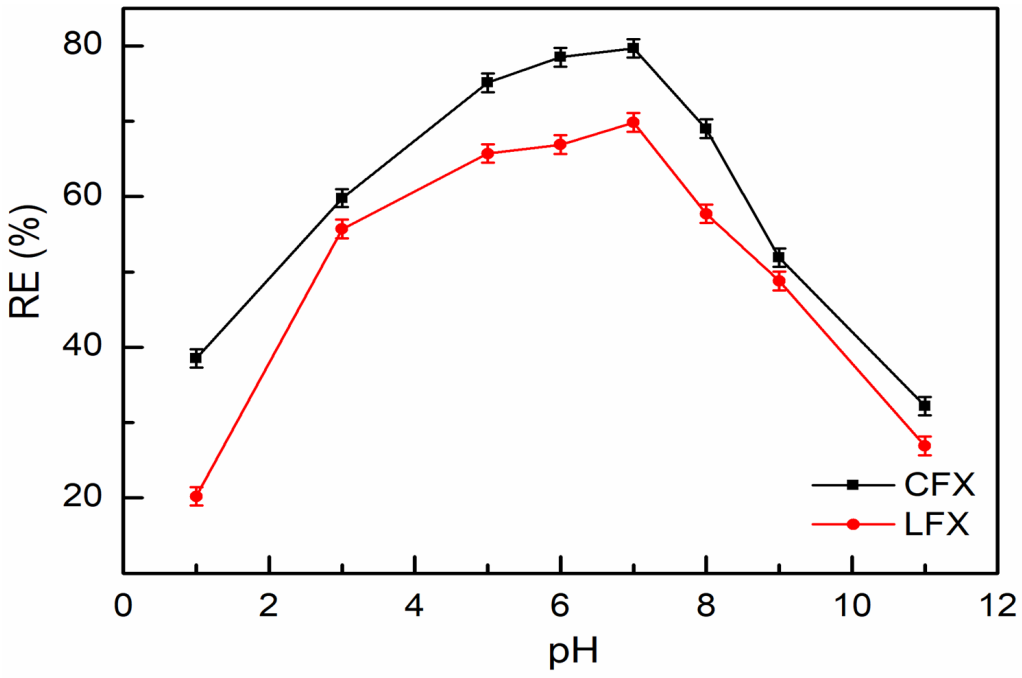

Figure 8. Effect of pH on the removal efficiency of CFX and LFX (experimental conditions: m (CS-MNPs) = 20 mg, V = 25 mL, C_0 = 10.15 mg/L, time = 30 min, and T = 293 K, n = 3).

3.2.3. Effect of Initial Concentration and Contact Time

When comparing the effectiveness of this adsorbent to other adsorbents, it is necessary to consider the amount of time needed to reach equilibrium in the solution to be treated and the initial concentration of the adsorbent. At initial concentrations of 2.51–15.07 mg/L and 2.53–15.11 mg/L of CFX and LFX, respectively, the effects of CS-MNP exposure time were examined. The outcomes are displayed in Figure 9. The trend of the curves for CFX and LFX adsorption on CS-MNPs may be found to be similar. The removal percentages for both antibiotics increased significantly over the first 40 min. The trend of increasing percentage removal of CFX and LFX was maintained after 60 min, albeit with a less steep slope. The resulting curves in this period were almost parallel to the horizontal axis.

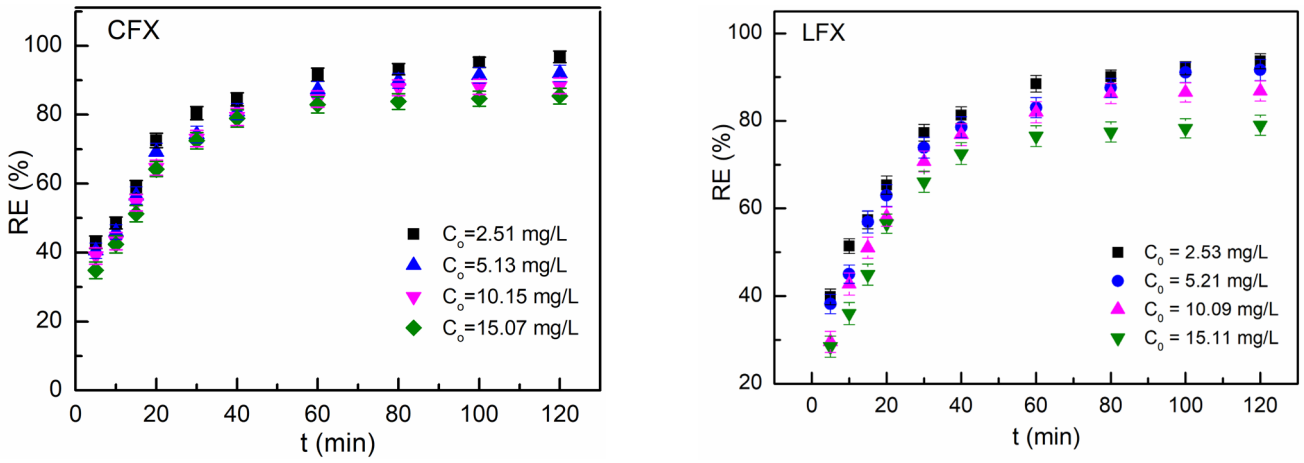

Figure 9. Effect of initial concentration of CFX, LFX, and adsorption time on adsorption efficiency (experimental conditions: m (CS-MNPs) = 20 mg, V = 25 mL, pH = 7, time = 5–120 min, and T = 293 K; n = 3).

Their ability to be removed from the solution decreased as the initial concentrations of CFX and LFX increased. The removal efficiencies of CFX after 120 min were 96.81, 92.01, 88.37, and 85.40%, respectively, corresponding to starting concentrations C_0 = 2.51, 5.13, 10.15, and 15.07 mg/L. And, the LFX removal efficiencies were 93.63, 91.62, 86.80, and 79.03%, corresponding to starting concentrations of C_0 of 2.53, 5.21, 10.09, and 15.11 mg/L, respectively. At all of the starting concentrations examined, these values were not significantly higher than the antibiotic removal efficiency at a previous time (t = 60, 80, or 100 min). Between the effective removal values at 60 and 120 min, there was a 4–5% error. Thus, the equilibration period for CFX and LFX was selected to be 60 min in order to guarantee adsorption efficiency and economy.

3.2.4. Effect of Adsorbent Dose

To accurately estimate the adsorption ability of the adsorbent, the adsorbent dosage is an important factor [40,52]. Figure 10 depicts the impact of CS-MNPs adsorbent dosage on CFX and LFX adsorption efficiency. It can be observed that the removal efficiency of the antibiotics CFX and LFX increases as the adsorbent dose rises from 0.5 to 2.0 g/L. This can be because when the CS-MNPs dose rose, the surface area and adsorption site of CS-MNP increased. The result of CFX and LFX were more absorbed. The removal efficiency still rose when the adsorbent dosage was between 0.75 and 2.0 g/L; however, there was not much difference in the adsorption efficiencies. The amount of adsorbent equal to 0.75 g/L (corresponding to the adsorbent mass of 20 mg) was selected for further studies to avoid the waste of adsorbent.

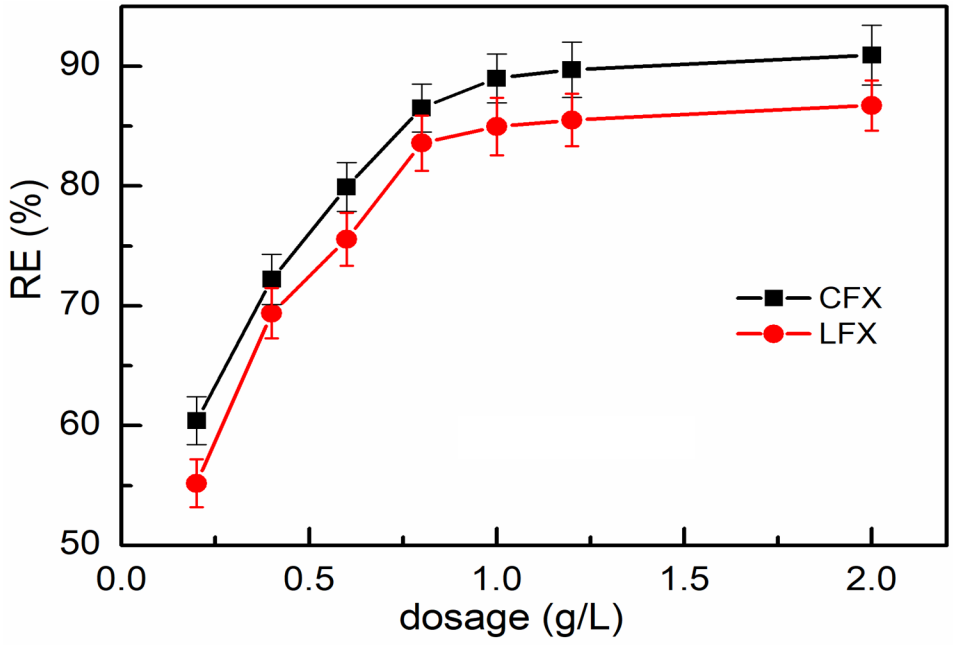

Figure 10. Effect of adsorbent dosage on adsorption efficiency (experimental conditions: $C_{0,CFX}$ = 10.21 mg/L, $C_{0,LFX}$ = 10.18 mg/L, m (CS-MNPs) = 5–50 mg, V = 25 mL, pH = 7, time = 60 min, and T = 293K; n = 3).

3.2.5. Adsorption Kinetic Models

The kinetics of CFX and LFX adsorption onto CS-MNPs were analyzed by pseudo-first-order and pseudo-second-order kinetic models [53]. Equations (4) and (5), respectively, describe the nonlinear version of the model.

$$q_t = q_e(1 - e^{-K_1 t}) \tag{4}$$

$$q_t = \frac{q_e^2 K_2 t}{1 + q_e K_2 t} \tag{5}$$

where K_1 (1/min) is the first-order adsorption rate constant, K_2 (g/mg·min) is the second-order adsorption rate constant, q_e (mg/g) is the adsorption capacity at equilibrium time.

The adsorption kinetic models in Figure 11 described how adsorption capacity varied over time. Table 3 includes the necessary parameters for the pseudo-first- and second-order kinetic models and statistical analysis variables. The correlation coefficient (R^2) was used with other statistical tools such as *MAE* (mean absolute error), *MSE* (mean square error), and *RMSE* (root mean square error) to determine the goodness of fit of the model (Equations (6)–(8)).

$$MAE = \frac{\sum_i^n \left| q_{e,\exp} - q_e \right|_i}{N} \tag{6}$$

$$MSE = \frac{\sum_i^n (q_{e,\exp} - q_e)_i^2}{N} \tag{7}$$

$$RMSE = \sqrt{\frac{\sum_i^n (q_{e,\exp} - q_e)_i^2}{N}} \tag{8}$$

where: $q_{e,exp}$ is the adsorption capacity at equilibrium time (t = 120 min), q_e is the adsorption capacity according to the model, and N is the number of data points.

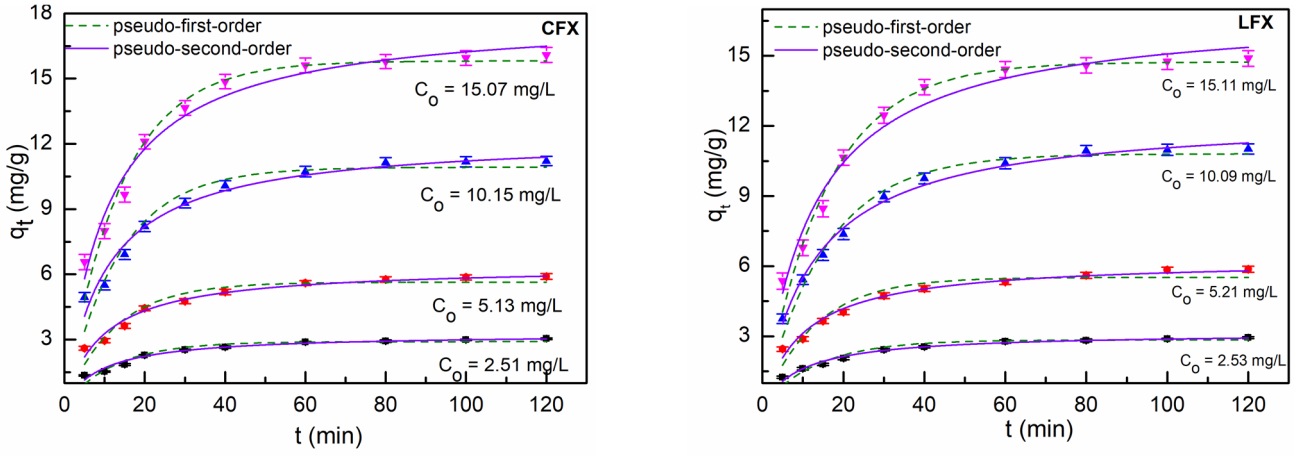

Figure 11. Adsorption kinetic of CFX and LFX onto CS-MNPs (experimental conditions: m (CS-MNPs) = 0.02 g, V = 25 mL, pH 7, time = 5–120 min, and T = 293 K, n = 3).

Table 3. The kinetic models' constants.

C_0 (mg/L)	Pseudo-First-Order			$q_{e,exp}$	Pseudo-Second-Order		
	K_1 (1/min)	q_e (mg/g)	Statistical Analysis		K_2 (g/mg·min)	q_e (mg/g)	Statistical Analysis
CFX							
2.51	0.08	2.82	R^2 = 0.912 *MAE* = 0.217 *MSE* = 0.047 *RMSE* = 0.218	3.04	0.03	3.22	R^2 = 0.963 *MAE* = 0.180 *MSE* = 0.033 *RMSE* = 0.181
5.13	0.08	5.50	R^2 = 0.908 *MAE* = 0.513 *MSE* = 0.265 *RMSE* = 0.515	6.01	0.02	6.35	R^2 = 0.964 *MAE* = 0.337 *MSE* = 0.114 *RMSE* = 0.338
10.15	0.07	10.66	R^2 = 0.926 *MAE* = 0.550 *MSE* = 0.400 *RMSE* = 0.633	11.21	0.80×10^{-2}	12.36	R^2 = 0.966 *MAE* = 0.147 *MSE* = 0.024 *RMSE* = 0.155
15.07	0.07	15.79	R^2 = 0.962 *MAE* = 1.157 *MSE* = 1.341 *RMSE* = 1.158	16.95	0.54×10^{-3}	17.83	R^2 = 0.970 *MAE* = 0.880 *MSE* = 0.780 *RMSE* = 0.883
LFX							
2.53	0.07	2.81	R^2 = 0.928 *MAE* = 0.127 *MSE* = 0.016 *RMSE* = 0.128	2.94	0.03	3.05	R^2 = 0.984 *MAE* = 0.113 *MSE* = 0.013 *RMSE* = 0.113
5.21	0.08	5.44	R^2 = 0.915 *MAE* = 0.540 *MSE* = 0.296 *RMSE* = 0.544	5.98	0.02	6.15	R^2 = 0.975 *MAE* = 0.173 *MSE* = 0.031 *RMSE* = 0.176
10.09	0.06	10.74	R^2 = 0.979 *MAE* = 0.350 *MSE* = 0.125 *RMSE* = 0.354	11.01	0.64×10^{-2}	11.19	R^2 = 0.992 *MAE* = 0.147 *MSE* = 0.047 *RMSE* = 0.217
15.11	0.05	14.74	R^2 = 0.979 *MAE* = 1.150 *MSE* = 1.323 *RMSE* = 1.150	15.89	0.14×10^{-2}	16.97	R^2 = 0.995 *MAE* = 1.080 *MSE* = 1.166 *RMSE* = 1.080

Table 3 shows that the correlation coefficient R^2 of the pseudo-first-order model was lower than the correlation coefficient of the pseudo-second-order model for all initial concentration values of CFX and LFX considered. The difference between the pseudo-first-order model's calculated adsorption capacity (q_e) and the experimental value ($q_{e,exp}$) was greater than it was for the pseudo-second-order model. The pseudo-second-order kinetic model's statistical analysis values were lower than those of the pseudo-first-order model. In other words, the pseudo-second-order model was better suited for the adsorption of CFX and LFX onto CS-MNPs. According to this model, the second-order kinetic reaction was addressed by the adsorption of CFX and LFX on CS-MNPs. The outcomes also confirmed that the rate constant decreased (K_2 = 0.03–0.54 × 10^{-3} g/mg·min for CFX and K_2 = 0.03–0.14 × 10^{-3} g/mg·min for LFX) as the initial concentrations of CFX and LFX rose ($C_{0,\,CFX}$ = 2.51–15.07 mg/L and $C_{0,LFX}$ = 2.53–15.11 mg/L). The results of other studies about the kinetics of antibiotic adsorption on adsorbents, such as kaolinite [54], tea leaf biochar [55], and magnetic nanoparticles, were likewise consistent with this one [19].

3.2.6. Adsorption Isotherm Models

In equilibrium studies, the Langmuir, Freundlich, and Temkin isotherm models were applied to fit the equilibrium data (Figure 12). The nonlinear mathematical expression of the Langmuir, Freundlich, and Temkin models are provided by Equations (9)–(11), respectively. The results of the parameters are presented in Table 4.

$$q_e = \frac{q_m K_L C_e}{(1 + K_L C_e)} \tag{9}$$

$$q_e = K_F C_e^{1/N_F} \tag{10}$$

$$q_e = \frac{RT}{B_T} \ln(K_T C_e) \tag{11}$$

where: q_m (mg/g) is the maximum adsorption capacity; K_L (L/mg) is Langmuir's constant; N_F is the Freundlich constant; K_F ($mg^{1-(1/n)}\ L^{1/n}/g$) is the adsorption parameter. If the N_F is in the range of $1 \div 10$, the Freundlich model is suitable for the adsorption process [56]; K_T (L/mg) is Temkin's constant; B_T (J/mol) is the adsorption energy; R = 8.314 (J/mol·K) is the gas constant; and T (K) is the absolute temperature.

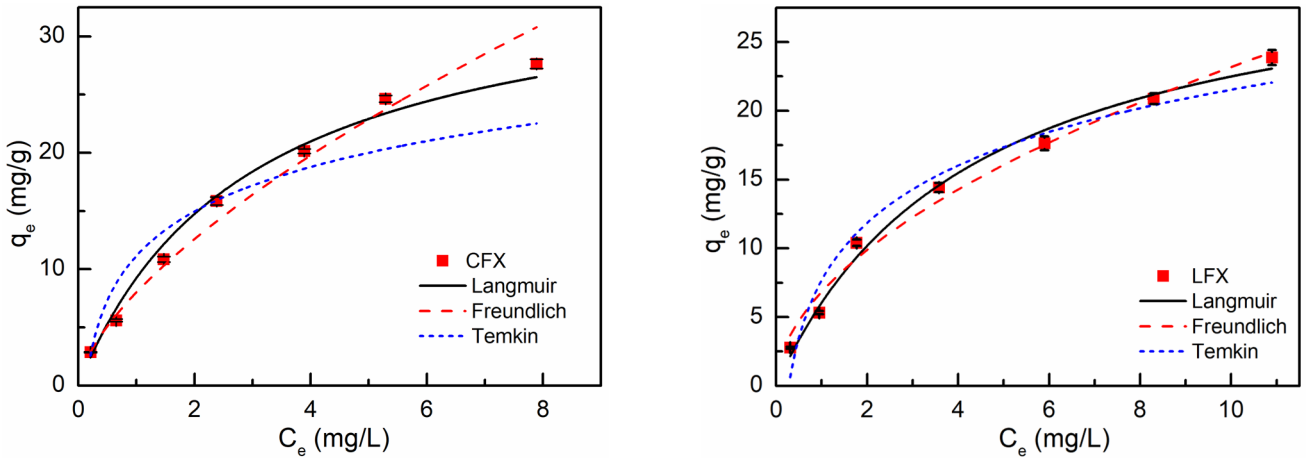

Figure 12. Adsorption isotherm models of CFX and LFX onto CS-MNPs (experimental conditions: m (CS-MNPs) = 20 mg, pH = 7, C_0 = 2.5–30 mg/L, V = 25 mL, time = 60 min, and T = 293 K, n = 3).

Table 4. The parameters of the adsorption model.

Pollutant	Langmuir Isotherm			
	q_m (mg/g)	K_L (L/g)	R_L	R^2
CFX	36.31	0.34	0.54–0.09	0.991
LFX	32.22	0.23	0.63–0.13	0.989
	Freundlich isotherm			
	N_F	K_F ($mg^{1-(1/n)}\ L^{1/n}/g$)		R^2
CFX	1.54	8.02		0.981
LFX	1.89	6.84		0.984
	Temkin isotherm			
	b_T (J/mol)	K_T (L/mg)		R^2
CFX	450.47	7.60		0.902
LFX	411.60	3.58		0.954

The coefficient R^2 of the CFX and LFX adsorption processes was calculated using the Langmuir model (R^2 = 0.991, 0.989), and this result was more significant than the Freundlich model (R^2 = 0.981, 0.984) and Temkin model (R^2 = 0.902, 0.954). Moreover, the R_L values for CFX and LFX ranged from 0.54 to 0.09 and 0.63 to 0.13 according to the formula: $R_L = 1/(1 + C_0. \times K_L)$. They all decreased below 1, demonstrating that the Langmuir model was appropriate for describing the adsorption of the antibiotics CFX and LFX on CS-MNPs [57]. Freundlich constants N_F = 1.54, 1.89 for CFX and LFX, respectively, were greater than 1, indicating a connection between the adsorbent and the CFX and LFX adsorbed [57]. As a result, these antibiotics' adsorption on CS-MNPs was more in line with the Langmuir model than the Freundlich and Temkin models. In the investigated concentration range, the maximum adsorption capacity of CFX was 36.31 mg/g, which was higher than LFX's maximum adsorption capacity (32.22 mg/g). This result shows that the CFX antibiotic was better absorbed by CS-MNPs compared to LFX.

Table 5 presents the other adsorbent materials' CFX and LFX adsorption capacities from previous research. The findings demonstrated that CFX and LFX had a better adsorption capacity on CS-MNPs than some of the other examined adsorbents. Compared to CS-MNPs, materials such as CNCs-GO, biochar/ferrite composites, GO, and date stone AC had a higher capacity to absorb CFX and LFX, but the adsorption period was too long (240 min [53,58], 12–24 h [11,57]). The CS-MNPs required 60 min to reach their adsorption equilibrium. When looking into practical applications, this influences economic worth. As a result, CS-MNPs were an appropriate material to study antibiotic treatment in aqueous solutions.

Table 5. Comparison of adsorption capacities of various adsorbents for CFX and LFX in aqueous solutions.

No.	Pollutant	Adsorbent	pH	Temp	Time	Adsorption Capacity (mg/g)	Ref.
1	CFX	MWCNT	Not given	25 °C	200 min	4.95	[10]
2	CFX	Kaonilite	3–4.5	25 °C	20 min	6.29	[54]
3	CFX	GO	5.0	NG	12 h	379	[11]
4	CFX	Dopa-CoF NPs-CIP	7.0	25 °C	30 min	16.53	[59]
5	CFX	Mela-CoF NPs	7.0	25 °C	30 min	14.04	[59]
6	LFX	Fe_3O_4	6.5	33 °C	240 min	6.85	[19]
7	LFX	CNCs-GO	4.0	25 °C	240 min	49.72	[58]
8	LFX	Biochar/ferrite composites	5.0	25 °C	240 min	55.50	[53]
9	LFX	Date stone AC	9.0	30 °C	24 h	100.38	[60]
10	LFX	Rice husk biochar	8.0	30 °C	24 h	4.99	[61]
11	LFX	Wood chip biochar	6.5	30 °C	24 h	7.22	[61]
12	CFX	CS-MNPS	6.0	20 °C	60 min	36.31	In this study
13	LFX		6.0	20 °C	60 min	32.22	

3.3. Binary Adsorption

3.3.1. Effect of Mutual Interference in Binary Solutions

Figure 13 illustrates the effectiveness of removing CFX from an aqueous solution when LFX was present at various CFX: LFX concentration ratios (1:0, 1:0.5, 1:1, and 1:2), and vice versa. The results showed that when increasing the concentration of LFX in the binary system (CFX: LFX) following the above concentration ratio ($C_{0,CFX}$ = 2.51 and 5.13 mg/L), the ability to remove CFX reduced from 90.44 to 66.14% and from 86.94 to 45.42%, respectively. As the initial concentration of CFX increased, the removal efficiency of CFX in solution decreased at the same concentration ratio of CFX: LFX. The CFX removal efficiency was 80.08% and 66.86%, respectively, when the initial CFX concentrations were 2.51 mg/L and 5.13 mg/L and the CFX: LFX concentration ratio was 1:1.

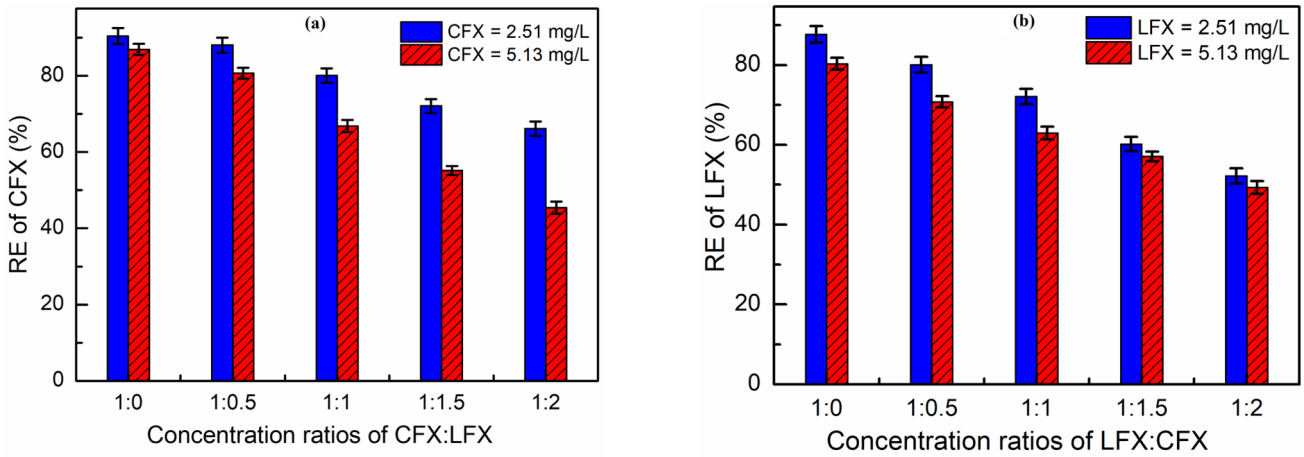

Figure 13. The efficiency of removing CFX (**a**) and LFX (**b**) from the binary system at different concentration ratios (experimental conditions: m (CS-MNPs) = 20 mg, V = 25 mL, time = 60 min, and T = 293 K; n = 3).

A similar result was seen when researching the impact of LFX in the presence of CFX in a binary system (LFX: CFX). When the amount of CFX in the system was increased, the ability to remove LFX fell from 87.65 to 52.19% and from 80.31 to 49.32%, respectively, corresponding to the initial concentrations of LFX of 2.51 mg/L and 5.13 mg/L. The LFX-removing efficiency was 72.11% and 62.96%, respectively, for the similar LFX: CFX concentration ratio of 1:1 and the initial LFX concentrations of 2.51 mg/L and 5.13 mg/L.

Consequently, it can be concluded that in a binary system, the first component's removal efficiency decreases when the second component is present, and the efficiency of component removal reduces as the initial concentration of these components increases. The same result was also obtained when studies were conducted to remove pollution components in binary systems such as diclofenac–paracetamol, ofloxacin–ciprofloxacin onto ZnO [62], levofloxacin–gemifloxacin onto granular silica pillared clay [63], ciprofloxacin–ofloxacin onto lignin-based adsorbents [42], and Cd-Pb onto chitosan/polymethacrylic acid/halloysite nanotube composite [64].

3.3.2. The Langmuir Competitive Model

The simultaneous adsorption of two antibiotics, CFX and LFX, was analyzed using the Langmuir competitive adsorption model (Figure 14). The competitive Langmuir model is an improved Langmuir model based on binary adsorption. The model mainly still considers the adsorption as monolayer adsorption. According to this hypothesis, only one adsorbent can hold an adsorption site [42,62,65,66] Equation (12) describes the competitive Langmuir model.

$$q_i = \frac{q_m \cdot b_i \cdot C_i}{1 + b_A \cdot C_A + b_B \cdot C_B} \quad (12)$$

The linear form of Equation (12) has the form:

$$\frac{C_A}{C_B \cdot q_A} = \frac{C_A}{q_{mA} \cdot C_B} + \frac{b_B}{b_A \cdot q_{mA}} \quad (13)$$

$$\frac{C_B}{C_A \cdot q_B} = \frac{C_B}{q_{mB} \cdot C_A} + \frac{b_A}{b_B \cdot q_{mB}} \quad (14)$$

where: C_A, C_B are the equilibrium concentrations of A, B (mg/L); q_A, q_B are the adsorption capacity of A, B at the equilibrium time (mg/g); q_{mi} is the maximum adsorption capacity of substance (i) in solution (mg/g); and $K_{LBA} = b_B/b_A$ and $K_{LAB} = b_A/b_B$ are parameters indicating heat of adsorption process [62,65,66].

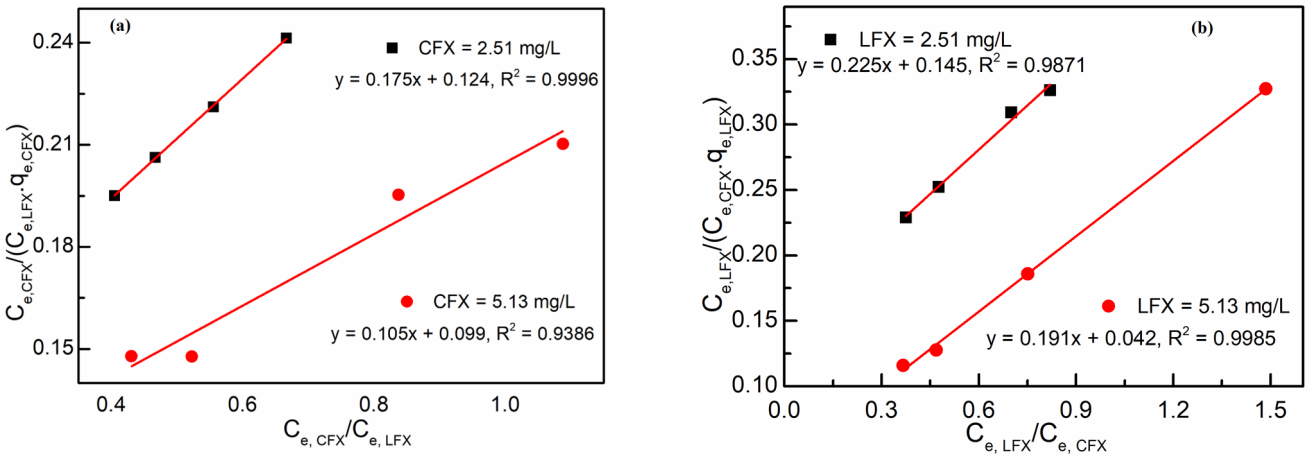

Figure 14. Langmuir competitive model for (**a**) ciprofloxacin: levofloxacin, (**b**) levofloxacin: ciprofloxacin (contact time 60 min, pH 7).

Table 6 shows the findings of calculating the parameters in the binary system model. The results indicated that the model's correlation coefficient is relatively high ($R^2 > 0.93$) for all initial concentrations of CFX and LFX. This demonstrated that the Langmuir competition model was suitable for describing the binary system (CFX: LFX) adsorption process onto CS-MNPs. The q_m values of CFX and LFX calculated from the model were lower than those calculated from the single system. The removal of each drug was thus decreased by the presence of the other when pharmaceuticals were present simultaneously in a binary solution, primarily due to competition between the adsorption sites on the adsorbent surface. Also, the findings of this study were in agreement with other previous studies on adsorption in binary systems [62,63,65–67].

Table 6. Langmuir competitive model parameters.

System	$C_{0,\,CFX}$ (mg/L)	$q_{m,\,CFX}$ (mg/g)	$K_{L,1} = b_{LFX}/b_{CFX}$	R^2
CFX:LFX	2.51	5.71	0.71	0.999
	5.13	9.52	0.94	0.939
	$C_{0,LFX}$ (mg/L)	$q_{m,\,LFX}$ (mg/g)	$K_{L,2} = b_{CFX}/b_{LFX}$	R^2
LFX:CFX	2.51	4.44	0.64	0.987
	5.13	5.24	0.22	0.998

3.4. Possible Mechanism of Adsorption

In actuality, chemisorption is related to the surface functional groups of adsorbents, whereas physisorption is connected with the structural characteristics of adsorbents. As a result, the structure and surface functional groups of adsorbents had a significant impact on the adsorption performance of adsorbents. Several adsorbent substrates can be suggested

(Figure 15) based on the structural properties of CS-MNPs and the experimental data of the adsorption process.

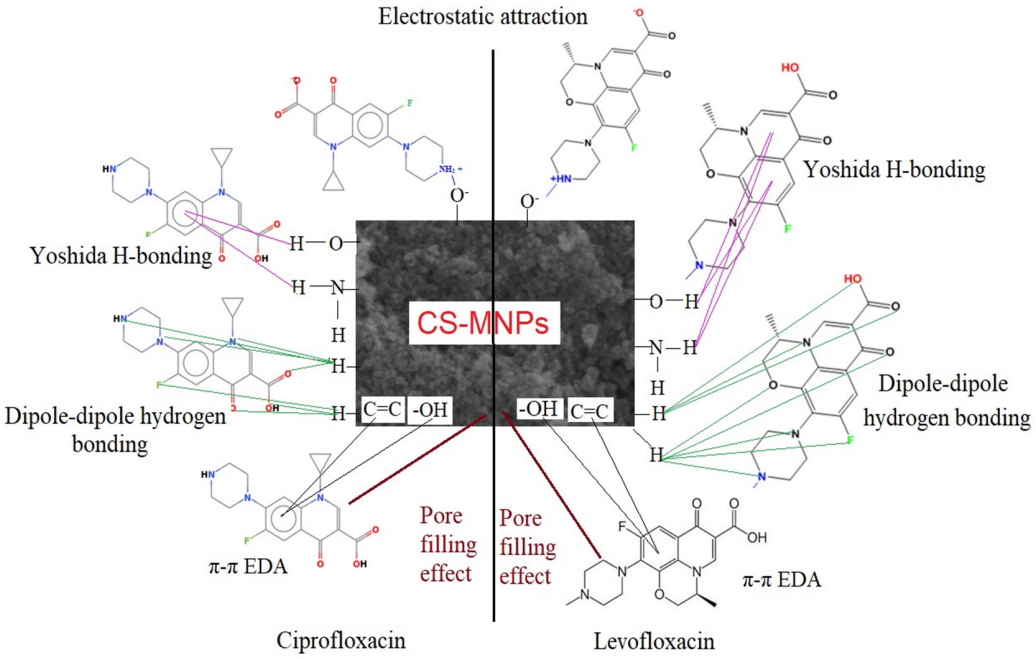

Figure 15. Schematic diagram of possible mechanisms of CFX and LFX adsorption onto the CS-MNPs.

Table 2 and Figure 4 show that CS-MNPs have porous surfaces, large surface areas, and large pore volumes. Therefore, the pore-filling effect could play an essential role in the physical adsorption of CFX and LFX on materials. In addition, when studying the impact of pH on the adsorption capacity, it can be seen that, at pH less than 6, when the surface of the material and the antibiotic were both positively charged, the removal efficiency of CFX and LFX reached 55–70%. This finding shows that, in addition to electrostatic interaction, physical adsorption with the pore-filling effect also contributed to removing antibiotics in water [21].

With the characteristics of functional groups in the material analyzed on the FTIR spectrum, it can be seen that chemical bonds may occur between CS-MNPs and CFX, LFC antibiotics. Numerous functional groups exist, including oxygen and hydrogen, in the antibiotic molecules and CS-MNPs adsorbents, so building hydrogen bonds and relying on hydrogen bonds to create adsorption is possible. Dipole–dipole hydrogen bonds and Yoshida hydrogen bonds are two types of hydrogen bonds that can occur. In addition to the Yoshida hydrogen bonding that can take place between the H of the -OH or -NH_2 group on the CS-MNPs surface and the aromatic rings of the antibiotics, the hydrogen on the CS-MNPs surface can also bond with the atoms of O, N, and F in the CFX and LFX structures via dipole–dipole hydrogen bonding [57,58,68]. Electron donor–acceptor (EDA) interaction is another possible action. When an organic molecule with an aromatic ring acts as the adsorbed species, EDA interaction may be one of the critical processes. Electron-rich and electron-poor entities interact in this way. The benzene ring in CFX and LFX can act as an electron acceptor, primarily because of the high electronegativity of the available fluorine group. Moreover, the hydroxyl group or the aromatic ring's C=C bond on the surface of CS-MNPs can function as an electron donor [57].

In summary, the adsorption mechanism of CFX and LFX antibiotics on CS-MNPs can include electrostatic interaction, pore-filling effect, π-π EDA, and hydrogen bonding, which can be vividly illustrated in Figure 15.

3.5. Reusability of CS-MNPs

Research on the reuse of adsorbents is an essential factor in environmental remediation applications because this helps with saving adsorbents and reducing secondary pollution. The CS-MNPs materials were separated from the solution by an external magnet and washed with 0.5 N NH_3 solution after the adsorption process. In this study, the reusability of CS-MNPs was investigated in four adsorption–desorption cycles. The results of CS-MNPs reuse in CFX and LFX antibiotic adsorption are shown in Figure 16. The results showed that the antibiotic removal efficiency after reusing CS-MNPs was slightly reduced compared to the starting material. After four recycling cycles, the CFX and LFX removal efficiency remained at 64.98 and 59.56%, respectively, indicating the high reuse potential of CS-MNPs. From these results, it can be shown that CS-MNPs have high stability, suitable adsorption capacity, and suitable regeneration performance to remove CFX or LFX from the aqueous.

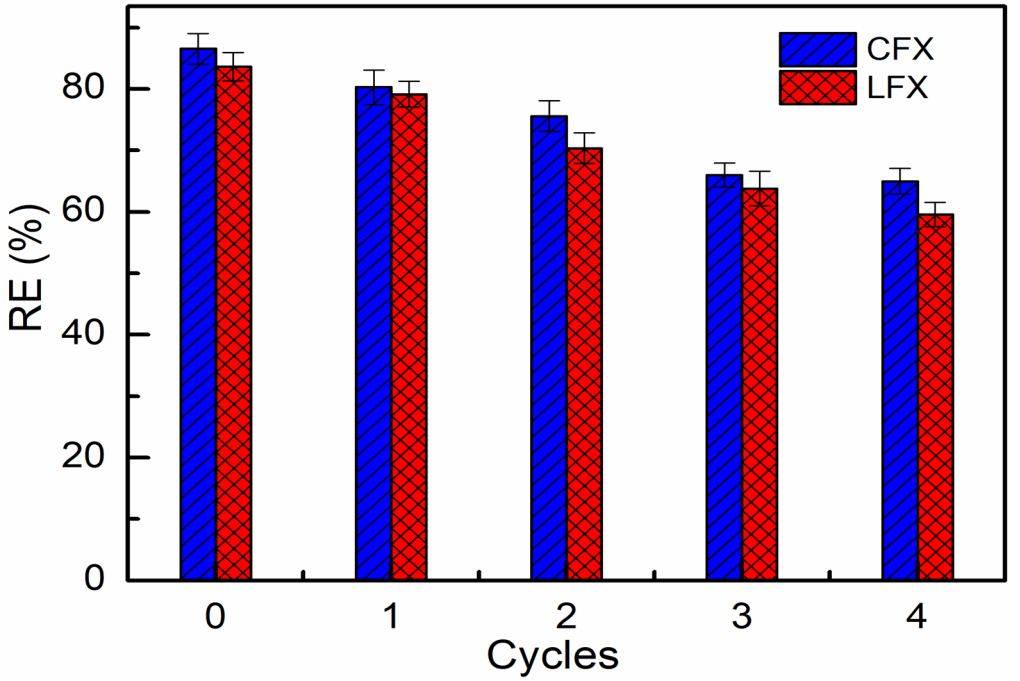

Figure 16. The reusability of the material (condition, desorption solution by 25 mL of NH_3 solution (0.5 N) for 60 min; adsorption, $C_{0,CFX}$ = 10.50 mg/L, $C_{0,LFX}$ = 10.86, t = 60 min, T = 293 K, and pH = 7, n = 3).

3.6. Application to Actual Samples

CFX- and LFX-contaminated wastewater samples of aquacultural farming from Thai Nguyen Province (in Northern Vietnam) were examined to determine the suitability of CS-MNPs as adsorbent. The sample was collected at 10–20 cm depth in March 2023. The water samples were stored in amber glass bottles at 4 °C in the dark and analyzed within 24 h. Table 7 summarizes the physicochemical properties of water, such as pH, dissolved oxygen (*DO*), and conductivity. Calcium, magnesium, and iron concentrations are also shown in the table. The concentrations of CFX and LFX in the samples were approximately 0.5–2.5 mg/L (Table 7). Under stirring for 60 min with 20 mg of CS-MNPs, CFX, and LFX were quantitatively removed from 25 mL of the sample (removal efficiency > 98%). These findings suggest that CS-MNPs are excellent candidates for removing CFX and LFX from aqueous solutions.

Table 7. Physicochemical properties and removal efficiency of CFX and LFX from actual samples.

Samples	Physicochemical Properties	C_{CFX} (mg/L)	*RE* (%)	C_{LFX} (mg/L)	*RE* (%)
S1	pH 7.4, conductivity: 135 µS/cm, *DO*: 5 mg/L, Ca 40 mg/L, Mg 8 mg/L, Fe 15 mg/L	2.05 ± 0.04	98.53 ± 2.20	1.37 ± 0.02	98.21 ± 2.30
S2	pH 7.7, conductivity: 226 µS/cm, *DO*: 3 mg/L, Ca 42 mg/L, Mg 10 mg/L, Fe 17 mg/L	0.51 ± 0.02	99.26 ± 2.56	0.98 ± 0.03	99.45 ± 3.20
S3	pH 7.6, conductivity: 319 µS/cm, *DO*: 4 mg/L, Ca 55 mg/L, Mg 12 mg/L, Fe 15 mg/L	0.94 ± 0.02	98.92 ± 2.42	2.12 ± 0.01	99.19 ± 1.50

4. Conclusions

The nanocomposite CS-MNPs were successfully synthesized by in situ combined co-precipitation. The synthesized CS-MNPs had a spinel-cubic crystal structure. The material existed in the sphere form with a diameter of about 20 nm and a surface area of 79.60 m^2/g. The material was highly magnetic, with a magnetic saturation value of 46.2 emu/g. CS-MNPs materials had suitable adsorption capacities for CFX and LFX antibiotics in an aqueous solution at pH 7, with a contact time of 60 min and an adsorbent dose of 20 mg. The adsorption processes were well described according to the Langmuir isotherm adsorption model. Maximum monolayer adsorption capacities for CFX and LFX were 36.31 mg/g and 32.22 mg/g, respectively. The kinetic data were best described by the pseudo-second-order model. CFX and LFX antibiotics can be adsorbed simultaneously in an aqueous solution using CS-MNPs. The efficiency of removing the first component from CS-MNPs materials depends on whether the second component was present in the binary system. In this binary system, the adsorption process followed the Langmuir competition model. Adsorption of CFX and LFX antibiotics on CS-MNPs was suggested by mechanisms including electrostatic interaction, pore-filling effect, π-π EDA, and hydrogen bonding. The synthesized CS-MNPs nanocomposite showed high stability and reusability over four adsorption–desorption cycles. The adsorption process was also applied to remove CFX and LFX from the actual wastewater samples. The results of this study demonstrated that CS-MNPs nanocomposite could be utilized in wastewater treatment processes.

Author Contributions: Writing—original draft preparation, Q.M.B. and. T.Q.V.; writing—review and editing, Q.M.B., X.T.V. and V.P.N.; conceptualization, L.T.N.N. and T.Q.V.; methodology, L.T.N.N. and V.D.N.; software, X.T.V. and V.D.N.; validation, Q.M.B. and V.P.N.; formal analysis, H.T.L.; investigation, T.Q.V. and H.T.H.N.; resources, H.T.L.; data curation, X.T.V. and H.T.H.N.; supervision, Q.M.B.; project administration, V.P.N. All authors have read and agreed to the published version of the manuscript.

Funding: This research was funded by TNU—University of Sciences in Vietnam, grant number CS2021-TN06-18.

Data Availability Statement: The authors confirm that the data supporting the findings of this study are available within the article.

Conflicts of Interest: The authors declare no conflict of interest.

References

1. Du, B.; Yang, Q.; Wang, R.; Wang, R.; Wang, Q.; Xin, Y. Evolution of Antibiotic Resistance and the Relationship between the Antibiotic Resistance Genes and Microbial Compositions under Long-Term Exposure to Tetracycline and Sulfamethoxazole. *Int. J. Environ. Res. Public Health* **2019**, *16*, 4681. [CrossRef]
2. Friedman, N.D.; Temkin, E.; Carmeli, Y. The negative impact of antibiotic resistance. *Clin. Microbiol. Infect.* **2016**, *22*, 416–422. [CrossRef]
3. Kraemer, S.A.; Ramachandran, A.; Perron, G.G. Antibiotic Pollution in the Environment: From Microbial Ecology to Public Policy. *Microorganisms* **2019**, *7*, 180. [CrossRef]
4. Carvalho, I.T.; Santos, L. Antibiotics in the aquatic environments: A review of the European scenario. *Environ. Int.* **2016**, *94*, 736–757. [CrossRef] [PubMed]

5. Fekadu, S.; Alemayehu, E.; Dewil, R.; Van der Bruggen, B. Pharmaceuticals in freshwater aquatic environments: A comparison of the African and European challenge. *Sci. Total Environ.* **2019**, *654*, 324–337. [CrossRef] [PubMed]
6. Li, Z.; Li, M.; Zhang, Z.; Li, P.; Zang, Y.; Liu, X. Antibiotics in aquatic environments of China: A review and meta-analysis. *Ecotoxicol. Environ. Saf.* **2020**, *199*, 110668. [CrossRef] [PubMed]
7. Binh, V.N.; Dang, N.; Anh, N.T.K.; Ky, L.X.; Thai, P.K. Antibiotics in the aquatic environment of Vietnam: Sources, concentrations, risk and control strategy. *Chemosphere* **2018**, *197*, 438–450. [CrossRef] [PubMed]
8. Liu, X.; Lu, S.; Guo, W.; Xi, B.; Wang, W. Antibiotics in the aquatic environments: A review of lakes, China. *Sci. Total Environ.* **2018**, *627*, 1195–1208. [CrossRef]
9. Szymańska, U.; Wiergowski, M.; Sołtyszewski, I.; Kuzemko, J.; Wiergowska, G.; Woźniak, M.K. Presence of antibiotics in the aquatic environment in Europe and their analytical monitoring: Recent trends and perspectives. *Microchem. J.* **2019**, *147*, 729–740. [CrossRef]
10. Baylan, N. Adsorption of cipro fl oxacin hydrochloride on multiwall carbon nanotube. *J. Mol. Struct.* **2020**, *1206*, 127711. [CrossRef]
11. Chen, H.; Gao, B.; Li, H. Removal of sulfamethoxazole and ciprofloxacin from aqueous solutions by graphene oxide. *J. Hazard. Mater.* **2015**, *282*, 201–207. [CrossRef]
12. Akhtar, J.; Amin, N.A.S.; Shahzad, K. A review on removal of pharmaceuticals from water by adsorption. *Desalin. Water Treat.* **2016**, *57*, 12842–12860. [CrossRef]
13. Yu, K.F.; Li, P.; Li, H.; Zhang, B.; Yang, J.; Huang, F.-Y.; Li, R.; He, Y. Potential of coagulation to remove particle-associated and free-living antibiotic resistome from wastewater. *J. Hazard. Mater.* **2021**, *406*, 124295. [CrossRef] [PubMed]
14. Liu, Q.; Hou, J.; Wu, J.; Miao, L.; You, G.; Ao, Y. Intimately coupled photocatalysis and biodegradation for effective simultaneous removal of sulfamethoxazole and COD from synthetic domestic wastewater. *J. Hazard. Mater.* **2022**, *423*, 127063. [CrossRef]
15. Taoufik, N.; Boumya, W.; Achak, M.; Sillanpää, M.; Barka, N. Comparative overview of advanced oxidation processes and biological approaches for the removal pharmaceuticals. *J. Environ. Manag.* **2021**, *288*, 112404. [CrossRef] [PubMed]
16. Bayan, E.M.; Pustovaya, L.E.; Volkova, M.G. Recent advances in TiO_2-based materials for photocatalytic degradation of antibiotics in aqueous systems. *Environ. Technol. Innov.* **2021**, *24*, 101822. [CrossRef]
17. Mao, Q.; Zhou, Y.; Yang, Y.; Zhang, J.; Liang, L.; Wang, H.; Luo, S.; Luo, L.; Jeyakumar, P.; Ok, Y.S.; et al. Experimental and theoretical aspects of biochar-supported nanoscale zero-valent iron activating H_2O_2 for ciprofloxacin removal from aqueous solution. *J. Hazard. Mater.* **2019**, *380*, 120848. [CrossRef]
18. Du, L.; Xu, W.; Liu, Y.; Li, X.; Huang, D.; Wu, S. Removal of Sulfamethoxazole in Aqueous Solutions by Iron-Based Advanced Oxidation Processes: Performances and Mechanisms. *Water Air Soil Pollut.* **2020**, *231*, 159. [CrossRef]
19. Al-Jabari, M.H.; Sulaiman, S.; Ali, S.; Barakat, R.; Mubarak, A.; Khan, S.A. Adsorption study of levofloxacin on reusable magnetic nanoparticles: Kinetics and antibacterial activity. *J. Mol. Liq.* **2019**, *291*, 111249. [CrossRef]
20. Kyzas, G.Z.; Fu, J.; Lazaridis, N.K.; Bikiaris, D.N.; Matis, K.A. New approaches on the removal of pharmaceuticals from wastewaters with adsorbent materials. *J. Mol. Liq.* **2015**, *209*, 87–93. [CrossRef]
21. Xiang, Y.; Xu, Z.; Zhou, Y.; Wei, Y.; Long, X.; He, Y.; Zhi, D.; Yang, J.; Luo, L. A sustainable ferromanganese biochar adsorbent for effective levofloxacin removal from aqueous medium. *Chemosphere* **2019**, *237*, 124464. [CrossRef]
22. Bakshi, P.S.; Selvakumar, D.; Kadirvelu, K.; Kumar, N.S. Chitosan as an environment friendly biomaterial—A review on recent modifications and applications. *Int. J. Biol. Macromol.* **2020**, *150*, 1072–1083. [CrossRef]
23. Rampino, A.; Borgogna, M.; Blasi, P.; Bellich, B.; Cesàro, A. Chitosan nanoparticles: Preparation, size evolution and stability. *Int. J. Pharm.* **2013**, *455*, 219–228. [CrossRef]
24. Saheed, I.O.; Da Oh, W.; Suah, F.B.M. Chitosan modifications for adsorption of pollutants—A review. *J. Hazard. Mater.* **2021**, *408*, 124889. [CrossRef] [PubMed]
25. Wan Ngah, W.S.; Teong, L.C.; Hanafiah, M. Adsorption of dyes and heavy metal ions by chitosan composites: A review. *Carbohydr. Polym.* **2011**, *83*, 1446–1456. [CrossRef]
26. Lyn, F.H.; Peng, T.C.; Ruzniza, M.Z.; Hanani, Z.N. Nur Hanani, Effect of oxidation degrees of graphene oxide (GO) on the structure and physical properties of chitosan/GO composite films. *Food Packag. Shelf Life* **2019**, *21*, 100373. [CrossRef]
27. Razzaz, A.; Ghorban, S.; Hosayni, L.; Irani, M.; Aliabadi, M. Chitosan nanofibers functionalized by TiO_2 nanoparticles for the removal of heavy metal ions. *J. Taiwan Inst. Chem. Eng.* **2016**, *58*, 333–343. [CrossRef]
28. Kadam, A.; Jang, J.; Lim, S.-R.; Lee, D.S. Low-Cost Magnetic Fe_3O_4/Chitosan Nanocomposites for Adsorptive Removal of Carcinogenic Diazo Dye. *Theor. Found. Chem. Eng.* **2020**, *54*, 655–663. [CrossRef]
29. Le, T.N.; Tran, T.D.; Kim, M.I. A Convenient Colorimetric Bacteria Detection Method Utilizing Chitosan-Coated Magnetic Nanoparticles. *Nanomaterials* **2020**, *10*, 92. [CrossRef]
30. Malakootian, M.; Nasiri, A.; Asadipour, A.; Faraji, M.; Kargar, E. A facile and green method for synthesis of $ZnFe_2O_4$@CMC as a new magnetic nanophotocatalyst for ciprofloxacin removal from aqueous media. *MethodsX* **2019**, *6*, 1575–1580. [CrossRef]
31. Wang, Y.; Yan, T.; Gao, L.; Cui, L.; Hu, L.; Yan, L.; Du, B.; Wei, Q. Magnetic hydroxypropyl chitosan functionalized graphene oxide as adsorbent for the removal of lead ions from aqueous solution. *Desalin. Water Treat.* **2016**, *57*, 3975–3984. [CrossRef]
32. Chang, Y.-C.; Chen, D.-H. Preparation and adsorption properties of monodisperse chitosan-bound Fe_3O_4 magnetic nanoparticles for removal of Cu(II) ions. *J. Colloid Interface Sci.* **2005**, *283*, 446–451. [CrossRef]

33. Erwin, A.; Salomo, S.; Adhy, P.; Utari, N.; Ayu, W.; Wita, Y.; Nani, S. Magnetic iron oxide particles (Fe_3O_4) fabricated by ball milling for improving the environmental quality. *IOP Conf. Ser. Mater. Sci. Eng.* **2020**, *845*, 12051. [CrossRef]
34. Huang, H.Y.; Shieh, Y.T.; Shih, C.M.; Twu, Y.K. Magnetic chitosan/iron (II, III) oxide nanoparticles prepared by spray-drying. *Carbohydr. Polym.* **2010**, *81*, 906–910. [CrossRef]
35. Panda, S.K.; Aggarwal, I.; Kumar, H.; Prasad, L.; Kumar, A.; Sharma, A.; Vo, D.-V.N.; Van Thuan, D.; Mishra, V. Magnetite nanoparticles as sorbents for dye removal: A review. *Environ. Chem. Lett.* **2021**, *19*, 2487–2525. [CrossRef]
36. Zulfikar, M.A.; Afrita, S.; Wahyuningrum, D.; Ledyastuti, M. Preparation of Fe_3O_4-chitosan hybrid nano-particles used for humic acid adsorption. *Environ. Nanotechnol. Monit. Manag.* **2016**, *6*, 64–75. [CrossRef]
37. Ashiq, A.; Vithanage, M.; Sarkar, B.; Kumar, M.; Bhatnagar, A.; Khan, E.; Xi, Y.; Ok, Y.S. Carbon-based adsorbents for fluoroquinolone removal from water and wastewater: A critical review. *Environ. Res.* **2021**, *197*, 111091. [CrossRef] [PubMed]
38. Mohammad, R.E.A.; Elbashir, A.A.; Karim, J.; Yahaya, N.; Rahim, N.Y.; Miskam, M. Adsorptive performances of magnetic graphene oxide adsorbent for the removal of fluoroquinolones in the Langat River Basin, Malaysia. *Int. J. Environ. Anal. Chem.* **2021**, 1–20. [CrossRef]
39. Pretali, L.; Fasani, E.; Sturini, M. Current advances on the photocatalytic degradation of fluoroquinolones: Photoreaction mechanism and environmental application. *Photochem. Photobiol. Sci.* **2022**, *21*, 899–912. [CrossRef]
40. Karimi-Maleh, H.; Ayati, A.; Davoodi, R.; Tanhaei, B.; Karimi, F.; Malekmohammadi, S.; Orooji, Y.; Fu, L.; Sillanpää, M. Recent advances in using of chitosan-based adsorbents for removal of pharmaceutical contaminants: A review. *J. Clean. Prod.* **2021**, *291*, 125880. [CrossRef]
41. Gao, B.; Chang, Q.; Cai, J.; Xi, Z.; Li, A.; Yang, H. Removal of fluoroquinolone antibiotics using actinia-shaped lignin-based adsorbents: Role of the length and distribution of branched-chains. *J. Hazard. Mater.* **2020**, *403*, 123603. [CrossRef]
42. Gao, B.; Chang, Q.; Yang, H. Selective adsorption of ofloxacin and ciprofloxacin from a binary system using lignin-based adsorbents: Quantitative analysis, adsorption mechanisms, and structure-activity relationship. *Sci. Total Environ.* **2021**, *765*, 144427. [CrossRef]
43. Bui, Q.M.; Nguyen, V.D.; Vu, T.Q.; Nguyen, L.T.N.; Nguyen, H.T.H. Removal of anionic dye from aqueous solution by chitosan—Magnetite nanocomposite. *Int. J. Environ. Anal. Chem.* **2022**, 1–21. [CrossRef]
44. Sureshkumar, V.; Daniel, S.C.G.K.; Ruckmani, K.; Sivakumar, M. Fabrication of chitosan–magnetite nanocomposite strip for chromium removal. *Appl. Nanosci.* **2016**, *6*, 277–285. [CrossRef]
45. Soares, P.I.; Machado, D.; Laia, C.; Pereira, L.C.; Coutinho, J.T.; Ferreira, I.M.; Novo, C.M.; Borges, J.P. Thermal and magnetic properties of chitosan-iron oxide nanoparticles. *Carbohydr. Polym.* **2016**, *149*, 382–390. [CrossRef]
46. Tomke, P.D.; Rathod, V.K. Facile fabrication of silver on magnetic nanocomposite (Fe_3O_4@Chitosan–AgNP nanocomposite) for catalytic reduction of anthropogenic pollutant and agricultural pathogens. *Int. J. Biol. Macromol.* **2020**, *149*, 989–999. [CrossRef]
47. Li, G.-Y.; Jiang, Y.-R.; Huang, K.-L.; Ding, P.; Chen, J. Preparation and properties of magnetic Fe3O4–chitosan nanoparticles. *J. Alloys Compd.* **2008**, *466*, 451–456. [CrossRef]
48. Rasoulzadeh, H.; Dehghani, M.H.; Mohammadi, A.S.; Karri, R.R.; Nabizadeh, R.; Nazmara, S.; Kim, K.-H.; Sahu, J. Parametric modelling of Pb(II) adsorption onto chitosan-coated Fe_3O_4 particles through RSM and DE hybrid evolutionary optimization framework. *J. Mol. Liq.* **2020**, *297*, 111893. [CrossRef]
49. Zheng, C.; Zheng, H.; Hu, C.; Wang, Y.; Wang, Y.; Zhao, C.; Ding, W.; Sun, Q. Structural design of magnetic biosorbents for the removal of ciprofloxacin from water. *Bioresour. Technol.* **2020**, *296*, 122288. [CrossRef]
50. Igberase, E.; Osifo, P.; Ofomaja, A. The adsorption of copper (II) ions by polyaniline graft chitosan beads from aqueous solution: Equilibrium, kinetic and desorption studies. *J. Environ. Chem. Eng.* **2014**, *2*, 362–369. [CrossRef]
51. Tewari, P.H.; McLean, A.W. Temperature dependence of point of zero charge of alumina and magnetite. *J. Colloid Interface Sci.* **1972**, *40*, 267–272. [CrossRef]
52. Nasiri, A.; Tamaddon, F.; Mosslemin, M.H.; Gharaghani, M.A.; Asadipour, A. New magnetic nanobiocomposite $CoFe_2O_4$ @methylcellulose: Facile synthesis, characterization, and photocatalytic degradation of metronidazole. *J. Mater. Sci. Mater. Electron.* **2019**, *30*, 8595–8610. [CrossRef]
53. Yao, B.; Luo, Z.; Du, S.; Yang, J.; Zhi, D.; Zhou, Y. Sustainable biochar/$MgFe_2O_4$ adsorbent for levofloxacin removal: Adsorption performances and mechanisms. *Bioresour. Technol.* **2021**, *340*, 125698. [CrossRef] [PubMed]
54. Li, Z.; Hong, H.; Liao, L.; Ackley, C.J.; Schulz, L.A.; Macdonald, R.A.; Mihelich, A.L.; Emard, S.M. A mechanistic study of ciprofloxacin removal by kaolinite. *Colloids Surf. B Biointerfaces* **2011**, *88*, 339–344. [CrossRef]
55. Li, J.; Yu, G.; Pan, L.; Li, C.; You, F.; Xie, S.; Wang, Y.; Ma, J.; Shang, X. Study of ciprofloxacin removal by biochar obtained from used tea leaves. *J. Environ. Sci.* **2018**, *73*, 20–30. [CrossRef]
56. de Luna, M.D.G.; Flores, E.D.; Genuino, D.A.D.; Futalan, C.M.; Wan, M.-W. Adsorption of Eriochrome Black T (EBT) dye using activated carbon prepared from waste rice hulls—Optimization, isotherm and kinetic studies. *J. Taiwan Inst. Chem. Eng.* **2013**, *44*, 646–653. [CrossRef]
57. Movasaghi, Z.; Yan, B.; Niu, C. Adsorption of ciprofloxacin from water by pretreated oat hulls: Equilibrium, kinetic, and thermodynamic studies. *Ind. Crops Prod.* **2018**, *127*, 237–250. [CrossRef]
58. Tao, J.; Yang, J.; Ma, C.; Li, J.; Du, K.; Wei, Z.; Chen, C.; Wang, Z.; Zhao, C.; Deng, X. Cellulose nanocrystals/graphene oxide composite for the adsorption and removal of levofloxacin hydrochloride antibiotic from aqueous solution: Nanocomposites adsorb antibiotics. *R. Soc. Open Sci.* **2020**, *7*, 200857. [CrossRef]

59. Malik, R.; Goyal, A.; Yadav, S.; Gupta, N.; Goel, N.; Kaushik, A.; Kumar, V.; Tikoo, K.B.; Singhal, S. Functionalized magnetic nanomaterials for rapid and effective adsorptive removal of fluoroquinolones: Comprehensive experimental cum computational investigations. *J. Hazard. Mater.* **2019**, *364*, 621–634. [CrossRef] [PubMed]
60. Darweesh, T.M.; Ahmed, M.J. Batch and fixed bed adsorption of levofloxacin on granular activated carbon from date (*Phoenix dactylifera* L.) stones by KOH chemical activation. *Environ. Toxicol. Pharmacol.* **2017**, *50*, 159–166. [CrossRef]
61. Yi, S.; Gao, B.; Sun, Y.; Wu, J.; Shi, X.; Wu, B.; Hu, X. Removal of levofloxacin from aqueous solution using rice-husk and wood-chip biochars. *Chemosphere* **2016**, *150*, 694–701. [CrossRef] [PubMed]
62. Dhiman, N.; Sharma, N. Removal of pharmaceutical drugs from binary mixtures by use of ZnO nanoparticles: (Competitive adsorption of drugs). *Environ. Technol. Innov.* **2019**, *15*, 100392. [CrossRef]
63. Farajfaed, S.; Sharifian, S.; Asasian-Kolur, N.; Sillanpää, M. Granular silica pillared clay for levofloxacin and gemifloxacin adsorption from aqueous systems. *J. Environ. Chem. Eng.* **2021**, *9*, 106306. [CrossRef]
64. Maity, J.; Ray, S.K. Chitosan based nano composite adsorbent—Synthesis, characterization and application for adsorption of binary mixtures of Pb(II) and Cd(II) from water. *Carbohydr. Polym.* **2018**, *182*, 159–171. [CrossRef]
65. Ni, B.J.; Huang, Q.S.; Wang, C.; Ni, T.Y.; Sun, J.; Wei, W. Competitive adsorption of heavy metals in aqueous solution onto biochar derived from anaerobically digested sludge. *Chemosphere* **2019**, *219*, 351–357. [CrossRef]
66. Abali, M.; Ichou, A.A.; Benhiti, R. Adsorption of Anionic Dyes Using Monoionic and Binary Systems: A Comparative Study. *Lett. Appl. NanoBioScience* **2021**, *10*, 2588–2593. [CrossRef]
67. Nharingo, T.; Ngwenya, T.J. Single and binary sorption of lead(II) and zinc(II) ions onto Eichhornia Crassipes (water hyacinth) ash. *Int. J. Eng. Sci. Innov. Technol.* **2013**, *2*, 419–426.
68. Singh, S.K.; Das, A. The n $\rightarrow \pi^*$ interaction: A rapidly emerging non-covalent interaction. *Phys. Chem. Chem. Phys.* **2015**, *17*, 9596–9612. [CrossRef] [PubMed]